JOURNAL OF SOLID STATE CHEMISTRY 4, 311–323 (1972)

Magnetic and Mössbauer Effect Studies of Mn_5Si_3:Fe_5Si_3 Solid Solutions

VANCLIFF JOHNSON, J. F. WEIHER, C. G. FREDERICK, AND D. B. ROGERS

Central Research Department, E. I. du Pont de Nemours and Company, Experimental Station, Wilmington, Delaware 19898*

Received June 23, 1971

For the entire series $Mn_{5-x}Fe_xSi_3$ ($x = 1, 2, 3, 3.5$, and 4) with the D_{8_8} structure, Mössbauer-effect measurements show Mn and Fe atoms preferentially occupy the $6(g)$ and $4(d)$ positions, respectively, with a small amount of disorder. Compositional dependence of the hexagonal lattice parameters and their ratio, c/a, correlate with these site preferences. Contrary to the findings of a previous study, these results do not suggest that this ordering varies with composition.

Relative magnitudes of the magnetic moments, $Fe_I[4(d)]:Fe_{II}[6(g)]$ and $Mn_I[4(d)]:Mn_{II}[6(g)]$, inferred from our Mössbauer and magnetic measurements and from previously reported data, are consistent with the Pauling valences of the respective metal atoms. A qualitative discussion of bonding in these phases emphasizing the importance of metal–metal bonding is given within the framework of MO theory.

Introduction

A large number of metal-rich, metalloid compounds belong to the general "filled" NiAs family of structures. Chemical bonding in these phases is transitional between that in ionic–covalent compounds and that in intermetallics. The chemistry of these compounds has not been extensively studied, the transitional bonding is not well understood, and the several structural variants that occur are not predictable. Further development of the crystal chemistry of these materials, therefore, seems worthwhile.

The immediate objective of this study was to determine site preferences and magnetic moments of the Mn and Fe atoms in the $Mn_{5-x}Fe_xSi_3$ system with the hexagonal $Mn_5Si_3(D_{8_8})$ structure. Mössbauer, magnetic, and cell-constant measurements have been performed on several members of the series and these are discussed in terms of chemical bonding.

Structure

The hexagonal Mn_5Si_3 structure is usually regarded as a "partially filled" NiAs structure (*1*). The octahedral sites in Mn_5Si_3 are two-thirds occupied and the trigonal bipyramidal sites completely so. Distortion from the ideal NiAs arrangement also occurs. The structure belongs to space group P_{6_3}/mcm with metal atoms in two inequivalent sites [$4M_I$ in $4(d)$; $6M_{II}$ in $6(g)$]. Distorted metalloid octahedra about the M_I atoms share faces along the c-axis, giving rows of M_I atoms along c (Fig. 1). The M_{II} metal atoms are surrounded by a severely distorted trigonal bipyramid of metalloid atoms, and have two close M_{II} neighbors in the same plane (Fig. 1) and three at somewhat larger distances in the planes above and below. The six closest M_{II} atoms form octahedra that share faces along c at each corner of the unit cell; octahedra at only two corners are shown in Fig. 1. Silicon atoms are coordinated by $4M_I$ atoms and $5M_{II}$ atoms in a distorted triangular prismatic arrangement.

Previous Work

Several Mössbauer-effect, neutron diffraction, and magnetic studies of the compounds Mn_5Si_3, Fe_5Si_3, and Mn_5Ge_3 with the Mn_5Si_3 structure have been reported. The results are summarized in Table I.

For Mn_5Ge_3, assignment of moments for Mn_I and Mn_{II} atoms is ambiguous. Ciszewski (*2*) and Forsyth and Brown (*3*), by neutron diffraction measurements, agree on the moment magnitudes but differ in their assignments (Table I). Average moments obtained from saturation magnetization and susceptibility measurements are consistent with each other and essentially agree with the neutron moments, but they do not give site assignments.

* Contribution No. 1736.

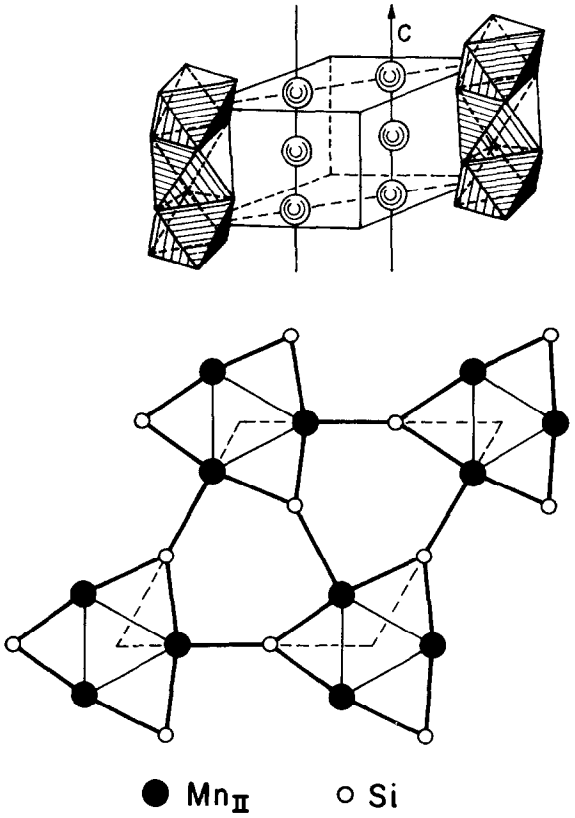

FIG. 1. Mn_5Si_3 Structure: Upper: Chains of 4(*d*) metal atoms and chains of octahedra formed by 6(*g*) metal atoms. Si atoms and octahedral chains at two corners of the unit cell are omitted. Lower: Plane of M_{II} and Si atoms projected along *c*. Similar planes above and below are rotated 60°.

In Fe_5Si_3 the magnetic hyperfine fields determined from Mössbauer-effect measurements by Shinjo et al. (*4*) are similar to those determined by Johnson et al. (*5*), but whereas the former assigned magnetic hyperfine fields of 235 kOe to Fe_I in 4(*d*) and 135 kOe to Fe_{II} in 6(*g*), Johnson et al. made the reverse assignment. The latter workers also found, from neutron diffraction, moments of $1.05\mu_B$ for Fe_I and $1.55\mu_B$ for Fe_{II}. Saturation magnetization measurements on Fe_5Si_3 have given moments of $1.2–1.27\mu_B$ in reasonable agreement with the average neutron moment of $1.35\mu_B$. However, the paramagnetic moment ($\mu_{eff} = 3.05\mu_B$) is somewhat larger.

For Mn_5Si_3 the observed paramagnetic moment, $\sim 3.9\mu_B$, (*6*, *7*) is also much larger than expected from the assigned neutron moments; $Mn_I = 0.4\mu_B$, $Mn_{II} = 1.2\mu_B$ (*8*). These neutron moments are much lower than those of isoelectronic and isostructural Mn_5Ge_3.

Experimental results for the silicides, particularly the magnetic moments of the inequivalent atoms, thus need clarification. Systematic study of the Mn_5Si_3:Fe_5Si_3 system should provide useful information.

Mössbauer-effect and magnetic studies of the Mn_5Si_3:Fe_5Si_3 system have recently been reported by Narasimhan, Reiff, Steinfink, and Collins (*9*) (NRSC hereinafter). Many of their results and conclusions differ considerably from ours. Differences will be discussed in the appropriate sections.

Experimental

Sample Preparation

Since Fe_5Si_3 is unstable below 800°C (it decomposes eutectoidally into Fe_3Si and FeSi) and since Mn has a relatively high vapor pressure at the melting point of the phases, the preparation of stoichiometric, single-phase specimens in the $Mn_{5-x}Fe_xSi_3$ system is difficult. Furthermore, phases with the Mn_5Si_3 structure can accommodate substantial amounts of *B*, *C*, *N*, or *O* in the centers of the octahedra formed by M_{II} atoms (Fig. 1); hence, rigorous exclusion of these probable contaminants is required (*13*).

Several $Mn_{5-x}Fe_xSi_3$ solid solutions with $0 \leqslant x < 5$ were prepared by a combination of induction melting and solid-state diffusion techniques. The purity of the elements (Mn from Metals Research Limited, Fe from United Mineral Corp., and Si from Texas Instruments) were claimed by the suppliers to be 99.99% or higher. Spectrographic analysis of the Mn revealed <20 ppm of other transition-metal atoms. The Mn was remelted by induction or arc melting and held well above its melting point to reduce oxide contamination. Pieces of the elements in the appropriate stoichiometry (excess Mn in empirically determined amounts was usually added) were prereacted by induction melting in outgassed Al_2O_3 crucibles (Morganite) under gettered argon or vacuum. The melts were cooled quickly to reduce segregation. Weight losses from the buttons were normally large (in most cases >1%) owing to the loss of Mn, which condensed on the cool, upper regions of the cylindrical crucibles. The buttons and Mn from the walls of the crucibles were weighed, and if necessary, the compositions adjusted under the assumption that the total weight loss was due to Mn. Samples were then powdered, sealed in silica tubes under vacuum, and fired for several days at subsolidus temperatures with intermediate grindings. All samples were annealed at 950°C and quenched; a few samples were also subsequently annealed at 750°C and furnace cooled.

TABLE I

MAGNETIC PROPERTIES OF BINARY D_{8_8} PHASES[d]

Compound	Magnetic order	T_c or T_n (°K)	μ_s (*B.M.*)	μ_{eff} (*B.M.*)	θ (°K)	μ_{M_I} (*B.M.*)	$\mu_{M_{II}}$ (*B.M.*)	H_{M_I} (kOe)	$H_{M_{II}}$ (kOe)
Fe_5Si_3	F	373(*4*) 381(*10, 11*) 385(*5*)[a]	1.2(*4*) 1.27(*10*)[b]	3.05 ± 0.03(*11*)[c]	546(*11*)	1.05 ± 0.15(*5*)	1.55 ± 0.15(*5*)	235(*4*) 137(*5*)	135(*4*) 180–242(*5*)
Mn_5Si_3	AF	68(*8*) 60(*6*)		3.9(*6*) 4.0(*7*)	 −50(*7*)	0.4 ± 0.1(*8*)	1.2 ± 0.1(*8*)		
Mn_5Ge_3	F	293(*12*) 300(*2*)	1.85(*12*) 2.35–2.50(*2*)	3.42(*12*) 3.5(*7*)	335(*12*) 300(*7*)	3.0 ± 0.1(*2*) 1.7 ± 0.1(*3*)	2.0 ± 0.1(*2*) 2.7 ± 0.1(*3*)		

[a] Sample studied was carbon stabilized.
[b] For sample with 37 at .% Si.
[c] For sample with 37.7 at. % Si.
[d] References given in brackets.

Phase Analysis and Cell Parameter Determination

Guinier–Hägg photographs (Cr radiation with 5 hr exposures) were used to check for neighboring phases. Several preparations contained small amounts of (Fe,Mn)Si and $(Fe,Mn)_3Si$ solid solutions. However, samples used for magnetic and Mössbauer studies were single phase. *d*-Spacings were obtained from Guinier–Hägg photographs (Cu radiation) with KCl as internal standard and cell parameters were refined by a least-squares computer program.

Magnetic Measurements

Magnetization and susceptibility between liquid helium temperature and 400°K were measured using a Foner-type vibrating sample magnetometer. High-temperature magnetic susceptibilities were measured with a Faraday balance.

Mössbauer Measurements

Mössbauer spectra at various temperatures were obtained using a modified Nuclear Science Instruments AM-1 constant acceleration drive. A 6mCi ^{57}Co in copper source was cooled or heated with the absorber. The Fe metal was used for velocity and isomer shift calibration. Spectra were fit with a least-squares computer program assuming Lorentzian line shapes.

Results

Lattice Parameters

Lattice parameters are given in Table II and shown in Fig. 2 as a function of composition. Of interest is the faster relative increase of the *a*-axis with respect to *c* as Mn is initially substituted for Fe and a reverse in this trend at higher Mn concentrations. This trend is also shown in Fig. 2 as the *c*/*a* ratio, which goes through a rather broad minimum, while the cell volume shows a nearly linear increase. The cell constants in Table II and their compositional dependence agree with those of Arönsson (*14*), but, with the exception of Mn_5Si_3, differ markedly from those of NRSC. Their cell constants for Mn_4FeSi_3, $Mn_3Fe_2Si_3$, and $Mn_2Fe_3Si_3$ were identical within their stated error limits. Since in their final step they melted and cooled over the short space of 2 hr, they probably had a range of compositions for each nominal one. Such ranges necessarily result on freezing intermediates in this system and can only be minimized by subsolidus annealing for much longer time periods.

Because of the affinity of these phases for interstitial contaminants and since oxide sample containers were used, an oxygen analysis was performed for Mn_4FeSi_3—the composition considered most susceptible to oxidation. An upper limit of 0.14 wt % oxygen was indicated, which, if present in the M_{II} octahedra of the D_{8_8} structure, would correspond to the composition $Mn_4FeSi_3O_{0.032}$ or 3.2 % of the M_{II} octahedral sites occupied by oxygen. This concentration of oxygen would affect the environment of approximately 6 % of the 6(*g*) metal atoms and may very well account for the seeming inequivalence of atoms in these positions. This will be discussed later. Similar inequivalences for 6(*g*) atoms have also been observed for Mn_5Si_3 (*8*) and Fe_5Si_3 (*5*).

For compositions Mn_4FeSi_3 and $Mn_3Fe_2Si_3$, the ratio Mn/Fe was determined by X-ray fluorescence

TABLE II

Mn_5Si_3:Fe_5Si_3 COMPOSITIONS–LATTICE PARAMETERS[a]

Composition	a(Å)	c(Å)	V(Å^3)	c/a	Annealing T(°C)	Cooling
Mn_5Si_3	6.9110(5)	4.8162(8)	199.2	0.696_9	950	Q[b]
Mn_4FeSi_3	6.8840(6)	4.7876(8)	196.5	0.695_5	950	Q
$Mn_3Fe_2Si_3$	6.8602(6)	4.7598(9)	194.0	0.693_8	950	Q
$Mn_2Fe_3Si_3$	6.8322(9)	4.7426(11)	191.7	0.694_2	950	Q
$Mn_{1.5}Fe_{3.5}Si_3$	6.8178(4)	4.7360(5)	190.6	0.694_6	950	Q
$MnFe_4Si_3$	6.8004(5)	4.7298(8)	189.4	0.695_5	950	Q
$Mn_3Fe_2Si_3$	6.8587(3)	4.7601(5)	193.9	0.694_0	750	S.C.[c]
$Mn_2Fe_3Si_3$	6.8335(7)	4.7418(8)	191.8	0.693_9	750	S.C.

[a] Numbers in brackets are uncertainties in the fourth place obtained in the refinements; they do not include systematic errors.

[b] Q: Quench.

[c] S.C.: Slowly cooled.

spectroscopy with respect to $Mn_2Fe_3Si_3$. The ratios obtained, 3.96 ± 0.05 for Mn_4FeSi_3 and 1.52 ± 0.05 for $Mn_3Fe_2Si_3$, show close correspondence to the nominal compositions of these preparations.

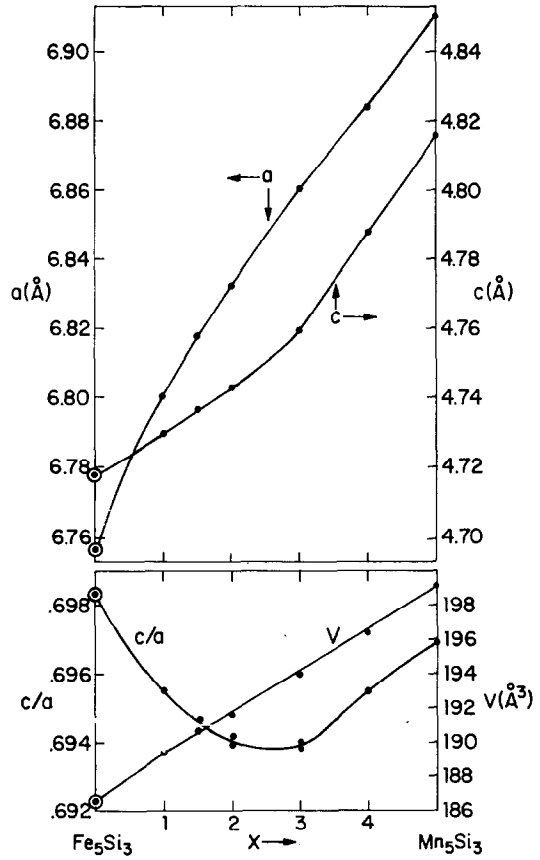

FIG. 2. $Mn_{5-x}Fe_xSi_3$: Cell constants, volume and c/a *vs.* composition.

Mössbauer Effect

In the Mn_5Si_3 structure two inequivalent metal sites are present, 4(d) with four positions and 6(g) with six positions in the unit cell. Throughout the range $Mn_{5-x}Fe_xSi_3$ ($x = 1$, 2, 3, 3.5, and 4) the Mössbauer spectra above the magnetic ordering temperatures were sums of two quadrupole-split pairs (Fig. 3) and below the ordering temperature, the sum of two six-line magnetic hyperfine patterns (Fig. 4). This suggests two types of iron atoms, which, from the crystal structure of Mn_5Si_3, we identify as Fe in 4(d), Fe_I, and in 6(g), Fe_{II}, sites. As the total iron content is increased, an increasing absorption by iron in one site relative to the other is observed (Fig. 3). For a completely random distribution of Fe atoms between the 4(d) and 6(g) sites, the absorption ratio would be constant throughout; hence, Fe preferentially occupies one site.

The relative intensity of absorption for each spectrum that could be unambiguously analyzed as two sites is listed in Table III. In general, the magnitude of the Mössbauer effect for a given amount of ^{57}Fe is a complex function of the sample temperature and the Mössbauer temperature, which is a parameter analogous to and often similar in magnitude to the Debye temperature. Since the Mössbauer temperature is related to Fe binding strength and since significant differences in that binding may be expected for the two sites, it would be dangerous to assume, *a priori*, that this parameter is the same for iron in both sites. However, the absorption ratio at low temperature is within the experimental error of that at high temperature for the two samples in which significant amounts of both types of iron are present. Thus, the Mössbauer temperatures of the two types of iron are probably

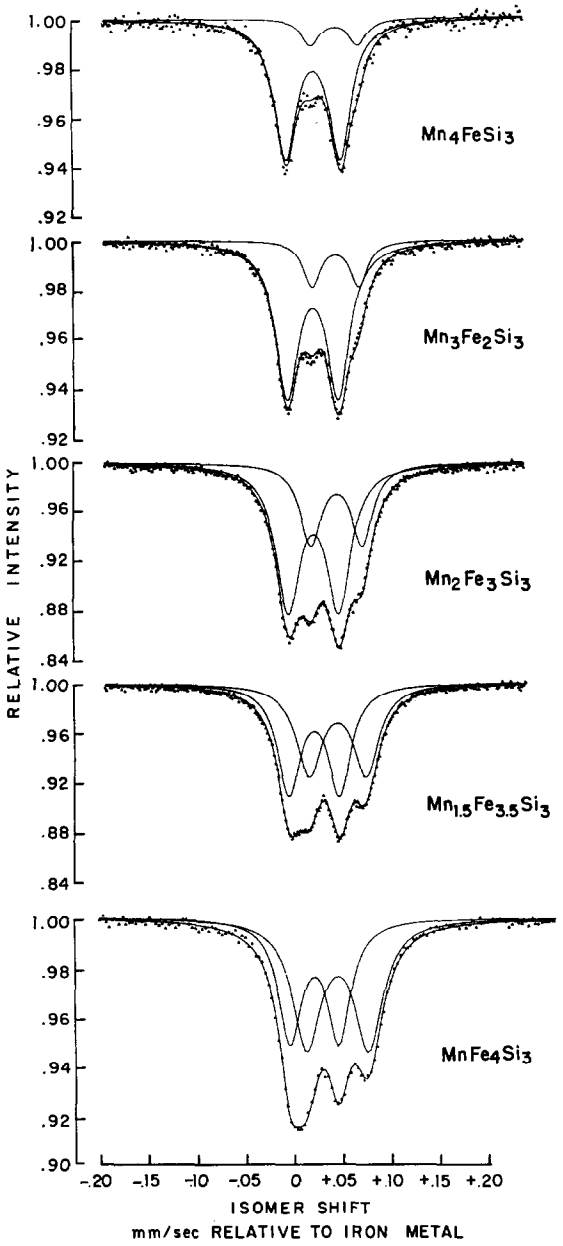

FIG. 3. Least-squares fits to Mössbauer spectra above the magnetic ordering temperatures; $MnFe_4Si_3$ at 350°K; all others at 298°K.

similar. Where this assumption is valid, the relative intensities, Table III, are a reliable estimate of the relative population of iron in the two sites. Site assignment of the respective absorptions was made on the basis of this intensity data.

The composition whose Mössbauer effect is most sensitive to site preference of Fe is $MnFe_4Si_3$. If Fe completely occupies 4(*d*) first, distribution would be $[4(d)]_2[6(g)]_2$ or an intensity ratio of 1:1; if 6(*g*) first, $[4(d)]_1[6(g)]_3$ or 1:3. Visual comparison of the observed spectrum for this composition with spectra calculated according to these two models (Fig. 5) clearly shows that the 4(*d*) site is preferentially occupied by Fe atoms. Therefore, the more intense quadrupole pair observed in the low Fe compositions (Fig. 3) is assigned to Fe in this site. Calculated and observed intensity ratios for 6(*g*) and 4(*d*) preferential occupation are also shown in Table III. Clearly, the experimental values more closely fit those calculated on the basis of 4(*d*) preferential occupation; however, the observation of two absorptions at all compositions shows the order is not perfect.

The degree of iron disorder over the two sites is uniquely described by the disorder parameter, *p* (*15*), which may be defined as

$$p = x_2(1 - x_1)/x_1(1 - x_2); \qquad x_i = CT_i M/m_i,$$

where T_i is the fractional population of the *i*th site, m_i is the number of *i* sites in the unit cell, *M* is the number of metal sites, and *C* is the iron concentration (mole fraction of metal). Taking 4(*d*) as $i = 1$ and 6(*g*) as $i = 2$, perfect order gives $p = 0$ and a completely random distribution gives $p = 1$. The values calculated for the disorder parameter from the observed intensity data of all pure quadrupole spectra, Table III, show that the degree of disorder is low. It is also not drastically temperature dependent since for $Mn_2Fe_3Si_3$ similar intensity ratios were observed for samples annealed at 950 and 750°C.

Isomer shifts and quadrupole splittings are given in Table IV. The constant isomer shift and the relatively constant quadrupole splitting for each site show that the two sites are unique throughout the composition range. Small changes in quadrupole splitting with composition may reflect small distortions from the site symmetries of the pure binaries as the other metal is progressively introduced. The electric field gradient decreases at the 4(*d*) site and increases at the 6(*g*) site as the Fe content is increased. This is consistent with the ordering scheme deduced previously, since the environment of a 4(*d*) Fe atom should become more symmetric as these positions approach complete occupation by Fe atoms. Conversely, the 6(*g*) Fe environments are initially uniform (all Mn atoms) at low Fe concentrations and progressively become less uniform as more Fe atoms enter 6(*g*). Uniform environments in this sense are of course expected for Fe_5Si_3.

The constancy of the shifts of iron in both sites suggests that the basic electronic configuration of iron, as reflected in the electron density at the

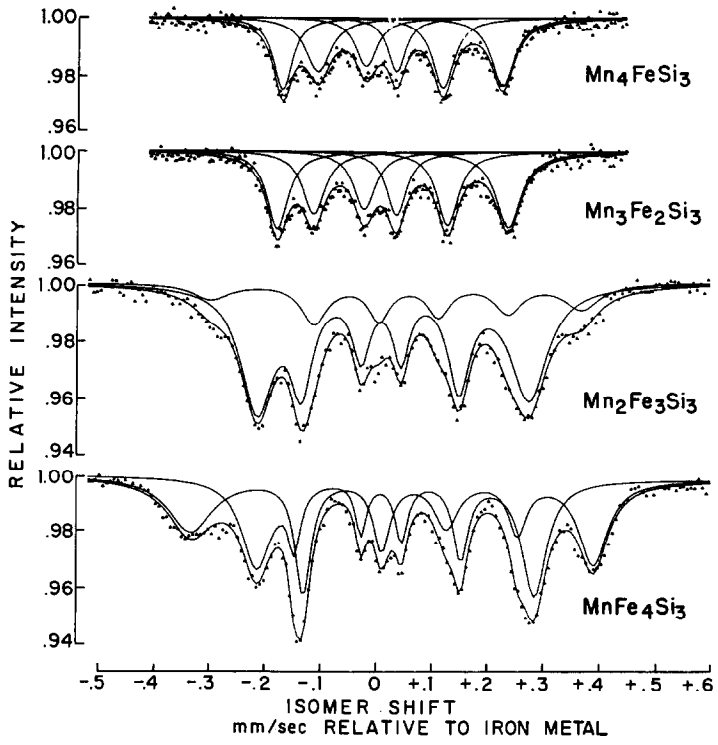

FIG. 4. Least-squares fits to Mössbauer spectra at 4.2°K.

nucleus, changes very little. Since covalency decreases the isomer shift, while increasing number of d electrons increases it, the observed isomer shifts for $Fe_I[4(d)]$ and $Fe_{II}[6(g)]$ are not inconsistent with the plausible *formal* valencies: $Fe^{III}[4(d)]$, $Fe^{II}[6(g)]$.

The magnitude of the magnetic hyperfine fields at liquid helium temperature, Table IV, increases with increasing Fe content for both $4(d)$ and $6(g)$ sites, with $4(d)$ always smaller. The magnetic hyperfine data is not sufficiently precise to determine the electric field gradient and its orientation with respect

TABLE III

Mn_5Si_3 : Fe_5Si_3 : RELATIVE MÖSSBAUER ABSORPTION AND DISORDER PARAMETER

Composition	Observed intensity[a] $\left[\frac{4(d)}{4(d)+6(g)}\right]^b$	Calculated intensity for perfect order $\frac{4(d)}{4(d)+6(g)}$	Calculated intensity for perfect order $\frac{6(g)}{4(d)+6(g)}$	Disorder parameter, p
Mn_4FeSi_3	0.83	1.0	1.0	0.085
$Mn_3Fe_2Si_3$	0.75	1.0	1.0	0.067
$Mn_2Fe_3Si_3$	0.63 (0.75)	0.67	1.0	0.034
$Mn_{1.5}Fe_{3.5}Si_3$	0.55	0.57	0.86	0.044
$MnFe_4Si_3$	0.49 (0.53)	0.50	0.75	0.043

[a] Intensity of pure quadrupole spectra (±0.05); values in brackets refer to magnetic hyperfine spectra (±0.11).

[b] Ratios obtained assuming this assignment of the absorptions.

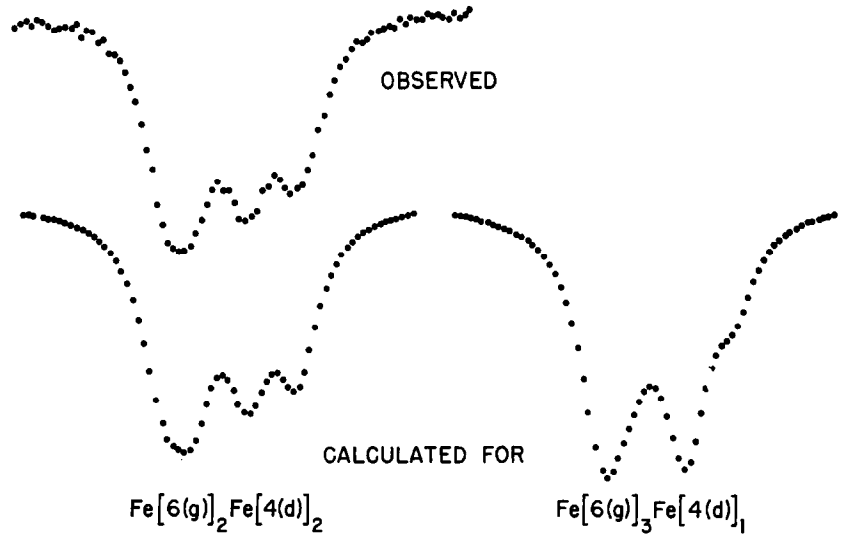

FIG. 5. Sensitivity of Mössbauer effect to site preference for $MnFe_4Si_3$.

to the hyperfine field, but the varying ratio, $(\gamma_6 - \gamma_5) - (\gamma_2 - \gamma_1)$, to the observed quadrupole splitting at high temperature, reflects changes in magnitude and orientation with Fe concentration.

At or above room temperature the line width for iron in the 4(*d*) site is constant, $\Gamma = 0.29 \pm 0.02$ mm/sec, throughout the composition range. This indicates very little difference in the 4(*d*) type iron in the unit cell and throughout the sample. The line width for Fe in 6(*g*) sites, however, increases monotonically from 0.21 ± 0.02 mm/sec for Mn_4FeSi_3 to 0.36 ± 0.02 mm/sec for $MnFe_4Si_3$. This increasing width suggests a range of environments for Fe in this site. At low temperatures, the much broader magnetic hyperfine lines for Fe in the 6(*g*) site also suggest such a variation. These observations suggest that the 6(*g*) sites are not quite equivalent in the solid solutions.

Isomer shifts, quadrupole splittings, hyperfine fields and line widths obtained in this study are in essential agreement with those observed by NRSC, who previously studied this system by Mössbauer

TABLE IV

Mn_5Si_3:Fe_5Si_3 SOLID SOLUTIONS: MÖSSBAUER HYPERFINE DATA

Composition	Temperature (°K)	Isomer shifts[a] (mm/sec ± 0.01)		Quadrupole Splittings (mm/sec ± 0.01)		$(\gamma_6 - \gamma_5) - (\gamma_2 - \gamma_1)$[c]		Magnetic hyperfine fields (kOe ± 15)	
		Fe 4(*d*)	Fe 6(*g*)	Fe 4(*d*)	Fe 6(*g*)	Fe 4(*d*)	Fe 6(*g*)	Fe 4(*d*)	Fe 6(*g*)
Mn_4FeSi_3	300	0.22	0.45	0.56	0.49	—	—	—	—
	4.2	0.20	—	—	—	+0.45	—	122	—
$Mn_3Fe_2Si_3$	300	0.21	0.44	0.54	0.50	—	—	—	—
	4.2	0.19	—	—	—	+0.45	—	130	—
$Mn_2Fe_3Si_3$	300	0.20	0.45	0.52	0.53	—	—	—	—
	4.2	0.19	0.48[b]	—	—	+0.47	−0.55	153	195
$Mn_{1.5}Fe_{3.5}Si_3$	300	0.20	0.44	0.53	0.59	—	—	—	—
$MnFe_4Si_3$	350	0.19	0.44	0.51	0.65	—	—	—	—
	4.2	0.17	0.43[b]	—	—	+0.66	−0.68	160	215

[a] Relative to iron metal.

[b] Larger experimental error (±0.03) due to complexity and overlap of spectra.

[c] For axially symmetric *EFG* $(\gamma_6 - \gamma_5) - (\gamma_2 - \gamma_1) = 1/2 \text{ eq } Q(3\cos^2\theta - 1)$, where θ is the angle between H and the *EFG* axis.

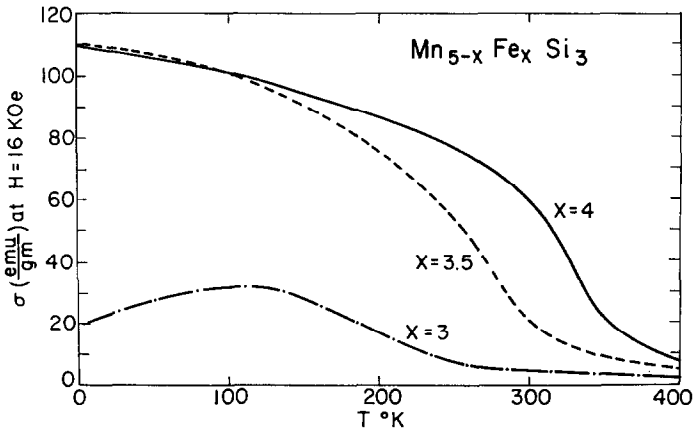

FIG. 6. $Mn_{5-x}Fe_xSi_3$: Magnetization *vs.* temperature.

spectroscopy. These parameters are greatly influenced by the site occupied by the Fe atom, but are only weakly affected by differences in composition. On the other hand, relative intensities of the two absorptions 4(*d*) and 6(*g*) ought to be very sensitive to composition. In fact, the relative intensities found by us are drastically different from those found by NRSC. This is no doubt due to differences in specimen homogeneities.

Magnetism

Compositions $MnFe_4Si_3$ and $Mn_{1.5}Fe_{3.5}Si_3$ are ferromagnetic (Fig. 6). With increasing Mn substitution T_c decreases, while the ferromagnetic moment (Table V) increases. The average moment for $MnFe_4Si_3$ of 1.44 μ_B/atom is larger than that of NRSC (1.11 μ_B); it is also larger than the average moment obtained by Johnson et al. (1.35 μ_B) (*5*) from neutron diffraction measurements on $Fe_5Si_3C_x$. From the Mössbauer results Mn preferentially occupies the 6(*g*) position, hence 6(*g*) Mn carries a larger moment than does 6(*g*) Fe. Assuming ferromagnetic order and the neutron moments of 1 μ_B and 1.5 μ_B obtained by Johnson et al. (*5*) for Fe in 4(*d*) and 6(*g*), respectively, we estimate the moment of 6(*g*) Mn to be 2.2 μ_B for both $MnFe_4Si_3$ and $Mn_{1.5}Fe_{3.5}Si_3$. This moment is substantially larger than the 1.2 μ_B for 6(*g*) Mn obtained by Lander et al. (*8*) from neutron diffraction studies of Mn_5Si_3.

TABLE V

Mn_5Si_3:Fe_5Si_3—MAGNETIC DATA

Composition	T_c(°K)	θ(°K)	μ_s (μ_B/atom)	μ_{eff} (μ_B/atom)
Mn_4FeSi_3	—	−12	—	4.05
$Mn_3Fe_2Si_3$	—	76	—	3.77
$Mn_2Fe_3Si_3$	—	215		3.66
$Mn_{1.5}Fe_{3.5}Si_3$	245	311	1.51	3.52
$MnFe_4Si_3$	315(5)	386	1.44	3.44

$Mn_2Fe_3Si_3$ is probably metamagnetic since σ goes through a field-dependent maximum (110°K at 16 kOe, 130°K at 300 Oe) as a function of temperature (Fig. 6). On the other hand, $Mn_3Fe_2Si_3$ and $Mn_4Fe_2Si_3$ are basically antiferromagnetic (Fig. 7), though both exhibit a residual moment and nonlinear field dependence of σ at liquid-helium temperature.

As Mn is initially substituted for Fe in the 6(*g*) site, it apparently aligns parallel to the Fe moment in this site. Upon complete occupation of the 6(*g*) site by Mn (at $Mn_3Fe_2Si_3$), antiferromagnetic order occurs in both 4(*d*) and 6(*g*) sites in view of the small residual moment observed at low temperature for $Mn_3Fe_2Si_3$ and Mn_4FeSi_4.

Paramagnetic data for the solid solutions are shown in Fig. 7 and Table V. In all cases, paramagnetic moments, μ_{eff}, from Curie–Weiss approximations to the susceptibility data are high with respect to the ferromagnetic moments. Such discrepancies are common in metallic phases and are not well understood; hence, very little can be inferred from these data concerning the electronic configuration of the transition-metal atoms.

Discussion

Lattice Parameters and Ordering Scheme

The Mössbauer-effect results for the $Mn_{5-x}Fe_xSi_3$ system indicate that Fe preferentially occupies the 4(*d*) position and Mn the 6(*g*) position across the entire series; however, they also indicate a small

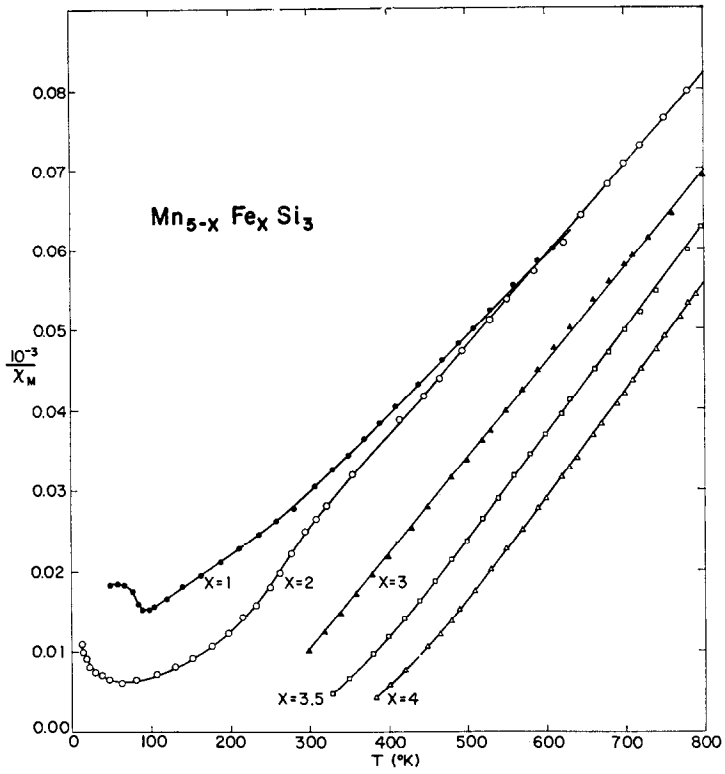

FIG. 7. $Mn_{5-x}Fe_xSi_3$: Reciprocal susceptibility *vs.* temperature.

amount of disorder. NRSC's ordering scheme, which indicates an inversion of site preferences at intermediate compositions, is not confirmed; our spectra are more consistent with the simpler picture of preferential occupation of 6(*g*) and 4(*d*) by Mn and Fe, respectively, for all compositions.

The ordering scheme we deduce from Mössbauer data explains the compositional dependence of lattice parameters for the system (Fig. 2). The M_I–M_I separations along the *c*-axis influence the *c* dimension most directly. The shorter these interatomic distances in the 4(*d*) metal atom chains (*c*/2) compared to the average interatomic distances in the structure, the smaller is the *c*/*a* ratio (*14*). As Mn is initially substituted for Fe, the *a*-axis shows a faster increase with respect to *c* (decreasing *c*/*a*). This is consistent with the smaller atom, Fe, preferentially occupying the 4(*d*) position. At the Mn-rich end of the series, *c* increases with respect to *a* as the larger atom, Mn, enters the 4(*d*) position. If the system were completely ordered and only size considerations significant, a smooth decrease in *c*/*a* to $Mn_3Fe_2Si_3$ and an increase thereafter would be anticipated. The rather broad minimum in *c*/*a*, therefore, suggests either incomplete order, as indicated by the Mössbauer effect, or subtle bonding or structural effects.

Ordering in the Ti_5Si_3:Mo_5Si_3 and Ti_5Si_3:W_5Si_3 systems have been determined by X-ray methods (*13*). The smaller and less electropositive Mo and W atoms substitute preferentially for Ti in the 4(*d*) position. Systematics for the Mn_5Si_3:Fe_5Si_3 system are similar; the small and less electropositive element, Fe, occupies the 4(*d*) position.

The more ionic phases with the NiAs structure possess *c*/*a* values close to 1.63 (*16*); this parameter decreases with increasing covalence. Phases with the Mn_5Si_3 structure have $c/a \simeq 1.4$, which suggests the covalent–metallic nature of the bonding. Furthermore, the M_I–M_I separations are short, indicating strong metal–metal bonding across the shared octahedral faces for the 4(*d*) position. Strong metal–silicon and metal–metal bonding are, therefore, simultaneously present in this structure. It has been emphasized (*16*) that metal-rich NiAs structures are more frequently encountered in metalloid compounds with small electronegativity differences between metal and metalloid. In this case, the decreased cationic charge allows close approach of the metal atoms giving rise to *d*–*d* interactions that

contribute to the binding energy. Presence of both metal–silicon and metal–metal covalent bonding precludes prediction of site preferences on the basis of ligand field stabilization energies—an approach that is quite successful in more ionic compounds. However, the extremely close approach of metal atoms in 4(*d*) may well account for this site being preferentially occupied by the less electropositive atom.

Our deduced preferences allow unambiguous assignment of the magnetic hyperfine fields, H_{eff}, to the respective Fe atoms. In accordance with Johnson et al. (*5*) and NRSC, Fe_{II} in 6(*g*) possesses the larger hyperfine field. By neutron diffraction from $Fe_5Si_3C_x$ Johnson et al. (*5*) found moments for Fe_{II} and Fe_I in the same relative magnitudes as H_{eff}. Assuming the same relationship exists for the solid solutions, our results contradict the predictions of the Kanematsu scheme of bonding in D_{8_8} phases (*17*), which predicts

$$\mu(Fe_I) = 2\mu_B > \mu(Fe_{II}) = 1\mu_B.$$

Magnetic hyperfine fields for the $Mn_{5-x}Fe_xSi_3$ system found by us and by NRSC, therefore, suggest that the relative magnitudes of the moments for Fe_I and Fe_{II} are the same for the entire series; however, absolute values may change with composition. These changes, if present, are probably considerably less than $\pm 1\mu_B$. Furthermore, at all compositions in the series the 6(*g*) Fe absorption shows magnetic hyperfine splitting, so that, in disagreement with the results of NRSC, a set of "magnetically random" 6(*g*) sites cannot be inferred.

Bonding

Because coordination geometries and metal–metal bonding are complex in the D_{8_8} phases, it is difficult to arrive at simple models of bonding. Pauling (*18*, *19*) argued that the metallic bond is very closely related to the covalent electron-pair bond and that the effective valence of an atom may be estimated from the known interatomic distances by use of the equation:

$$D(n) = D(1) - 0.600\ \text{Å} \log n,$$

where $D(n)$ is the interatomic distance for bond number n, and $D(1)$ is the interatomic distance for bond number 1, i.e., the fully covalent electron-pair bond. The effective valence, v_p (Pauling valence), of an atom i is therefore (*20*):

$$(v_p)_i = \sum_{j=i}^{n} (\text{C.N.})_{ij} \exp-\{[D(n)_{ij} - D(1)_{ij}]/0.26\},$$

where (C.N.) is the coordination number of neighboring atoms. Interatomic distances for Mn_5Si_3 reported by Arönsson (*21*) and those determined for Fe_5Si_3 and Mn_5Ge_3 assuming the positional parameters for Mn_5Si_3, have been used to calculate v_p (Table VI) for the respective atoms in these phases. As found by Pauling and Soldate (*22*) for FeSi, the effective valence of Si in the D_{8_8} phases (as well as probably M_I and M_{II}) is overestimated by this simple method. However, since for a given atom, the larger v_p, the smaller is the magnetic moment (*23*, *24*), the effective valences found for Fe_I and Fe_{II} in Fe_5Si_3 do correlate with the magnitudes of the magnetic moments. This approach has been applied by Mori and Mitsui (*20*) to a large number of Mn compounds, and they find good correlation between v_p and measured magnetic moments. The Pauling valence method is of value since it apparently takes into account both metal–metal and metal–metalloid covalent bonding in an effective way; presumably, the degree of overlap of the wave functions on neighboring atoms is approximated by the exponential dependence of v_p on interatomic distance.

Lander and Brown (*25*) measured the electron density distribution in Mn_5Si_3 and found the number

TABLE VI

PAULING VALENCE OF ATOMS IN D_{8_8} PHASES

Phase	Atom	Coordination	$D(1)$	$(V_p)_i$	v_p
Mn_5Si_3	$Mn_I4(d)$	$2Mn_I$	2.34	1.53	
		$6Mn_{II}$	2.34	0.56	
		6Si	2.34	4.23	6.32
	$Mn_{II}6(g)$	$4Mn_I$	2.34	0.37	
		$6Mn_{II}$	2.34	0.76	
		5Si	2.34	2.63	3.76
	Si6(*g*)	$4Mn_I$	2.34	2.82	
		$5Mn_{II}$	2.34	2.73	5.55
Fe_5Si_3	$Fe_I4(d)$	$2Fe_I$	2.33	1.774	
		$6Fe_{II}$	2.33	0.672	
		6Si	2.34	5.322	7.768
	$Fe_{II}6(g)$	$4Fe_I$	2.33	0.448	
		$6Fe_{II}$	2.33	0.834	
		5Si	2.34	3.304	4.586
	Si6(*g*)	$4Fe_I$	2.34	3.548	
		$5Fe_{II}$	2.34	3.304	6.852
Mn_5Ge_3	Mn_I	$2Mn_I$	2.34	1.17	
		$6Mn_{II}$	2.34	0.39	
		6Ge	2.39	3.50	5.06
	Mn_{II}	$4M_I$	2.34	0.269	
		$6Mn_{II}$	2.34	0.416	
		5Ge	2.39	2.16	2.84
	Ge	$4Mn_I$	2.39	2.132	
		$5Mn_{II}$	2.39	2.16	4.29

of electrons within 1.2 Å of the atomic centers to be ~1.5 greater for Mn_{II} than for Mn_I. This is consistent with the data of Table VI in that $(v_p)_i$ for M_I, with respect to Si or Ge, is larger than for M_{II}. These results and the observed isomer shifts for Fe_I and Fe_{II} suggest *formal* valences: $(Mn,Fe)^{III}$ $4d$, $(Mn,Fe)^{II}$ $6(g)$, Si^{IV} $6(g)$. Recognizing an analogy to the B_{8_2} (Ni_2In) structure, in which all M_I sites are filled as well as the M_{II}, we can schematically write the valence formula $(M_I^{3+})_{0.67}(M_{II}^{2+})(Si^{4-})$, for D_{8_8} phases. It is then interesting to note that the filled B_{8_2} structure, for which the corresponding formula would be $(M_I^{2+})(M_{II}^{2+})(Si^{4+})$, is most common for normally *divalent* M_I ions, e.g., Co or Ni, whereas the D_{8_8} is most common for normally *trivalent* M_I ions, e.g., Ti, V, or Cr. Manganese and iron, for which divalent and trivalent states are about equally common, would be expected to be transitional, and indeed, both structural types are found for these elements. We do not mean to imply that the charges are real; as emphasized previously, the bonding in these structures is highly covalent and metallic. However, formal valences are helpful in estimating the effective number of electrons in the metal *d* bands. Thus, we assume that three electrons from each M_I metal (two per Si, since $M_I/Si = 2/3$), two from each M_{II}, and four from each Si are involved in normal covalent bonding to form a filled primarily *s–p* valence band with eight electrons for each formula unit $(M_I)_{0.67}M_{II}Si$. The effective number of *d* electrons left on the metal atoms are then five for Fe_I and Mn_{II}, six for Fe_{II}, and four for Mn_I.

In NiAs and Ni_2In the site symmetries for M_I and M_{II} are $\bar{3}m$ and $\bar{6}m2$, respectively. The *d*-wave functions in these symmetries are split into three distinct sets—$a_1{}^T$, e, and e^T [where the labels are those of Goodenough (*27*)]. The e and e^T sets are each doubly degenerate. By analogy, we would expect a similar splitting in the D_{8_8} structure except that distortions of the octahedral and trigonal bipyramidal symmetries probably further remove degeneracy of the two "e" sets. Ordering of the levels cannot be inferred simply from site symmetry; however, for the M_{II} site we would intuitively expect the $a_1{}^T$ orbital, which is directed towards apical silicon atoms, to have more antibonding (M_{II}–Si) character than the others and, so, to be destabilized. This is consistent with the observation by Lander and Brown (*25*) that paired electrons for Mn_{II} in Mn_5Si_3 are predominantly in the basal plane (e^T orbitals) while unpaired ones are in orbitals with projections along the *c*-axis ($a_1{}^T$ and/or e). Therefore, we will assume that orbitals of M_{II} increase in energy in the order $e^T < e < a_1{}^T$. For M_I, the situation is probably reversed since $a_1{}^T$ points toward neighboring, electropositive M_I atoms along the *c*-axis and presumably participates in strong metallic bonding; we would intuitively expect it to be most stable. This is consistent with an LCAO treatment of NiS (NiAs structure) by Tyler and Fry (*26*), who suggest $a_1{}^T < e < e_1{}^T$; we assume the same relative ordering.

In view of the short metal–metal distances in these structures, we will assume, as did Goodenough (*27*) and Tyler and Fry (*26*), that all *d* orbitals participate in metallic (or covalent) bonding so that they are transformed into (possibly narrow) bands of collective-electron states. The magnetism of the compositions, however, shows that electron–electron correlations cannot be neglected, so we assume that the bands are partially exchange split. The amount of splitting and, consequently, the magnitude of the moment in a partially filled band will decrease with increasing band width, which is determined by the strength of the metal–metal interactions. With these assumptions, we can construct the schematic, one-electron, energy band diagram for Mn_5Si_3 shown in Fig. 8. This diagram not only rationalizes the observed magnetism for the D_{8_8} compositions, but also accounts for the relative magnitude of M_I- *vs.* M_{II}-site moments.

In the figure, broad, primarily *s–p*, valence (bonding, σ) and conduction (antibonding, σ^*) bands are assumed to form by covalent interactions between Mn and Si. Since there are three Si atoms per formula unit, each contributing four orbitals with a spin degeneracy of 2 per orbital, each of these bands can accommodate 24 electrons. The valence band is filled by six electrons from two Mn_I atoms, six from three Mn_{II}, and twelve from three Si, as discussed previously. It is further assumed that the *d*-state manifold and the Fermi energy lie in the gap between the top of the valence and bottom of the conduction bands. The *d*-levels are ordered in the manner discussed above and metallic interactions are assumed to broaden them into bands of collective-electron states. To obtain approximate agreement with the observed magnetic moments, the bands are assumed to be exchange split by an energy Δex into bands of different spin, α and β. In all cases, the numbers in brackets are the products of atomic, orbital, and spin degeneracies. The resultant diagram is similar to that proposed by Goodenough (*27*) for manganese in MnAs.

With four *d*-electrons per Mn_I on the left side of the figure and Δex approximately as shown, the $a_1{}^T$-α and $a_1{}^T$-β bands are filled, the e-α nearly so, and the e-β nearly empty. Thus, the net moment

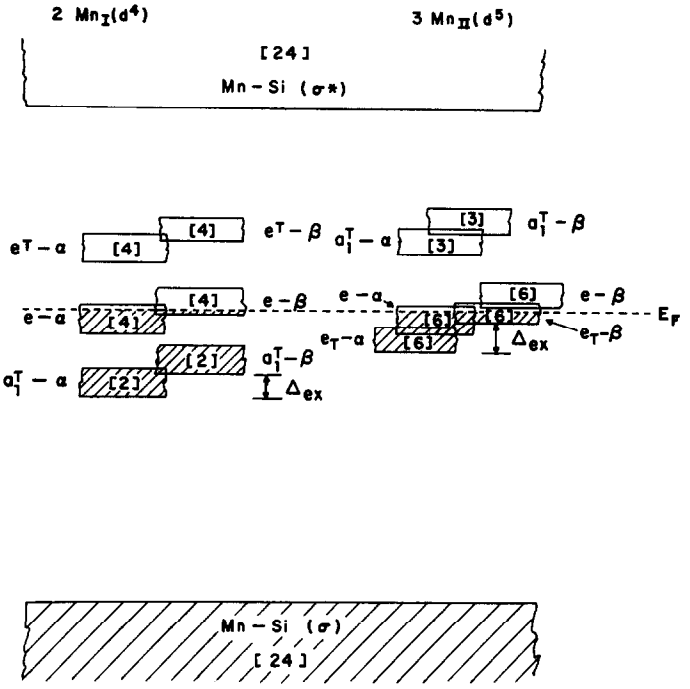

FIG. 8. Schematic MO energy-level diagrams for M_I and M_{II} atoms in D_{8_8} structure.

expected per Mn_I is somewhat less than $2\mu_B$. With five *d*-electrons per Mn_{II} on the right side, the e^T-α band is filled, the e-α nearly so, and the e^T-β somewhat more than half. The net moment expected for Mn_{II} is, therefore, somewhat less than $3\mu_B$. A similar treatment for Fe_5Si_3, with five *d*-electrons per Fe_I and six per Fe_{II}, gives $Fe_I \lesssim 1\mu_B$ and $Fe_{II} \lesssim 2\mu_B$.

Obviously, a diagram of the type shown in Fig. 8 can have only general, qualitative significance. For example, the σ bands may actually overlap the top and bottom of the *d*-state manifold, and the relative magnitudes both of band widths and of exchange splittings may be quite different from those shown. However, provided E_F is within the gap and the band ordering is approximately correct, the qualitative conclusions are preserved. These conclusions give relative moment magnitudes that are consistent with those observed. Perhaps of greater significance, the derived band scheme effectively illustrates the general features of the bonding in D_{8_8} phases.

Conclusions

Mn and Fe atoms preferentially occupy the 6(*g*) and 4(*d*) positions of the D_{8_8} structures in the $Mn_{5-x}Fe_xSi_3$ solid solution series. The site preferences are apparently related to the fact that the less electropositive atom, Fe, forms more stable metal–metal bonds in the 4(*d*) position than does Mn.

The Pauling-valencies of M_I and M_{II} atoms correlate with the relative magnitudes of the magnetic moments of these atoms. These moments do not agree with the predictions of the Kanematsu theory, but may be accounted for in terms of MO theory if formal valences of III for M_I and II for M_{II} are assumed.

References

1. F. JELLINEK, *Österr. Chem. Z.* **60**, 311 (1959).
2. R. CISZEWSKI, *Phys. Status Solidi* **3**, 1999 (1963).
3. J. B. FORSYTH AND P. J. BROWN, *Proc. Int. Conf. Magnetism* p. 524, Nottingham, England, 1964.
4. T. SHINJO, Y. NAKAMURA, AND N. SHIKAZONO, *J. Phys. Soc. Jap.* **18**, 797 (1963).
5. C. E. JOHNSON, J. B. FORSYTH, G. H. LANDER, AND P. J. BROWN, *J. Appl. Phys.* **39**, 465 (1968).
6. R. P. KRENTSIS, I. Z. RADOVSKII, P. V. GEL'D, AND L. P. ANDREEVA, *Russ. J. Inorg. Chem.* **10**, 1192 (1965).
7. K. VAN CON, *C.R. H. Acad. Sci.* **260**, 111 (1965).
8. G. H. LANDER, P. J. BROWN, AND J. B. FORSYTH, *Proc. Phys. Soc. (London)* **91**, 332 (1967).
9. K. S. V. L. NARASIMHAN, W. M. REIFF, H. STEINFINK, AND R. L. COLLINS, *J. Phys. Chem. Solids* **31**, 1511 (1970).
10. Y. LECOCQ, P. LECOCQ, AND A. MICHEL, *C.R. H. Acad. Sci.* **258**, 5655 (1964).

11. E. ÜBELACKER AND P. LECOCQ, *C.R. H. Acad. Sci. Ser.* **262**, 793 (1966).
12. R. FONTAINE AND R. PAUTHENET, *Compt. Rend.* **254**, 650 (1962).
13. E. PARTHE, W. JEITSCHKO, AND V. SADAGOPAN, *Acta. Crystallogr.* **19**, 1031 (1965).
14. B. ARÖNSSON, *Acta Chem. Scand.* **12**, 308 (1958).
15. S. S. HAFNER, "Development in Applied Spectroscopy," Vol. 8, p. 292, Plenum Press, NY (1970).
16. A. KJEKSHUS AND W. B. PEARSON, *Prog. Solid State Chem.* Vol. I, p. 89, Pergamon, Oxford (1964).
17. K. KANEMATSU, *J. Phys. Soc. Jap.* **17**, 85 (1962).
18. L. PAULING, *Acta Crystallogr. Ser. B* **24**, 5 (1968).
19. L. PAULING, *Phys. Rev.* **54**, 899 (1938).
20. N. MORI AND T. MITSUI, *J. Phys. Soc. Jap.* **25**, 82 (1968).
21. B. ARÖNNSON, *Acta Chem. Scand.* **14**, 1414 (1960).
22. L. PAULING AND A. M. SOLDATE, *Acta Crystallogr.* **1**, 212 (1948).
23. L. PAULING AND J. EWING, *Rev. Mod. Phys.* **20**, 112 (1948).
24. L. PAULING, "Quantum Theory of Atoms, Molecules and the Solid State" (P. Löwden, ed.), Academic, NY (1966).
25. G. H. LANDER AND P. J. BROWN, *Phil. Mag.* **16**, 521 (1967).
26. J. M. TYLER AND J. L. FRY, *Phys. Rev. B* **1**, 4604 (1970).
27. J. B. GOODENOUGH AND J. A. KAFALAS, *Phys. Rev.* **157**, 389 (1967).